Eur Biophys J (2007) 36:153–161
DOI 10.1007/s00249-006-0095-1

BIOPHYSICS LETTER

Quantitative detection of the ligand-dependent interaction between the androgen receptor and the co-activator, Tif2, in live cells using two color, two photon fluorescence cross-correlation spectroscopy

Tilman Rosales · Virginie Georget · Daniela Malide · Aleksandr Smirnov · Jianhua Xu · Christian Combs · Jay R. Knutson · Jean-Claude Nicolas · Catherine A. Royer

Received: 5 March 2006 / Revised: 31 July 2006 / Accepted: 25 August 2006 / Published online: 5 October 2006

Abstract Two-photon, two-color fluorescence cross-correlation spectroscopy (TPTCFCCS) was used to directly detect ligand-dependent interaction between an eCFP-fusion of the androgen receptor (eCFP-AR) and an eYFP fusion of the nuclear receptor co-activator, Tif2 (eYFP-Tif2) in live cells. As expected, these two proteins were co-localized in the nucleus in the presence of ligand. Analysis of the cross-correlation amplitude revealed that AR was on average 81% bound to Tif2 in the presence of agonist, whereas the fractional complex formation decreased to 56% in the presence of antagonist. Residual AR–Tif2 interaction in presence of antagonist is likely mediated by its ligand-independent activation function. These studies demonstrate that using TPTCFCCS it is possible to quantify ligand-dependent interaction of nuclear receptors with co-regulator partners in live cells, making possible a vast array of structure-function studies for these important transcriptional regulators.

T. Rosales · A. Smirnov · J. Xu · J. R. Knutson
Optical Spectroscopy - Section,
LBC, NHLBI, NIH, Bethesda,
MD 20892-1412, USA

V. Georget · J.-C. Nicolas
INSERM U540, Montpellier, France

D. Malide · C. Combs
NHLBI Light Microscopy Core Facility,
National Institutes of Health, Bethesda, MD, USA

C. A. Royer (✉)
INSERM U554, Montpellier, France
e-mail: royer@cbs.cnrs.fr

Introduction

Nuclear receptors (NRs) constitute a large family of ligand dependent transcriptional regulators. They represent one of the major molecular strategies for the control of development, differentiation, growth, and homeostasis in metazoans. Mutations or other malfunctions of the NR are implicated in a variety of human diseases including cancers (breast, prostate, uterine, and certain leukemias), cardiovascular disease and obesity, among others. Binding by agonist or antagonist ligands specifically and differentially influences the cellular localization of these receptors. Ligands also modify NR structural dynamics, thereby modulating their ability to interact with their cellular partners, such as molecular chaperones, DNA target sequences, and specific transcriptional co-regulators. For a recent review see (Nettles and Greene 2005). The androgen receptor (AR), a member of the steroid hormone receptor sub-family, mediates the role of androgens in male sexual development; certain mutations in the AR result in full or partial androgen insensitivity and incomplete development of the male sexual organs. Indeed, conditional knock-out studies demonstrated that the expression of AR in Sertoli cells is required for spermatogenesis (Chang et al. 2004; De Gendt et al. 2004). Moreover, abnormalities in AR function and interaction with co-regulators have been implicated in the development and progression of prostate cancer (Culig et al. 2004; Burnstein 2005; d'Ancona and Debruyne 2005; Edwards and Bartlett 2005a, b), and anti-androgens appear to be among the most promising therapeutic strategies in the treatment of the disease (d'Ancona and Debruyne 2005).

As with the other NRs, AR function is mediated by its interactions with transcriptional co-regulators, including the well-characterized p160 family of co-activators (SRC-1, Tif2/GRIP-1/SRC-2, and pCIP/RAC3/AIB1/ACTR/TRAM-1/SRC3), which exhibit histone acetyl transferase activity, allowing for the de-condensation of chromatin. These co-activators also recruit components of the general transcription machinery (Lonard and O'Malley 2005; Xu and Li 2003). Post-translational modifications and the expression levels of these co-regulators modulate the hormonal response in a tissue specific manner, thus allowing the integration of multiple signaling pathways (Lonard and O'Malley 2005; Smith and O'Malley 2004; Wu et al. 2005). The elucidation of the subtle structure-function relationships underlying ligand-dependent modulation of NR function will require direct quantification of the interactions between NRs and their cellular partners in an environment where (1) the full-length proteins can be used, (2) the role of post-translational modifications can be investigated, and (3) the effects of the expression levels of ternary partners and the impact of other factors (such as the cell cycle) can be assessed.

Two-photon, two-color fluorescence cross-correlation spectroscopy (TPTCFCCS) is a variation of single channel FCS and has been recently reviewed (Haustein and Schwille 2004; Bacia et al. 2006). In FCS one measures the fluctuations in fluorescence intensity that arise from molecular passages through a very small open volume defined by the confocal pinhole or the two-photon excitation probability. The most basic application of FCS, and that which is most useful in the study of bio-molecular associations, involves fluctuations due to the local changes in concentration (or number fluctuations). If one can arrange to excite simultaneously two fluorophores which emit at different wavelengths, and simultaneously detect their emission in two separate channels, it is possible to cross-correlate the intensity versus time traces. If the two fluorescent species are non-interacting and hence do not diffuse together, the fluctuations in intensity due to their number fluctuations will be entirely uncorrelated. If on the other hand, there is 100% complex formation, the fluctuations will be 100% correlated in time. Therefore, TPTCFCCS, in principle, can yield direct, very low background, quantitative measurements of protein–protein interactions in living cells because the cross correlation signal is null in absence of interactions.

TPTCFCCS was first applied to the study of bio-molecular interactions in vitro (Kettling et al. 1998). However, since the Scwhille group first measured cholera toxin subunit interactions after endocytosis in live cells by TCTPFCCS (Bacia et al. 2002), a very small number of other live cell applications (by that group and others) of TPTCFCCS, either based on fluorescent protein fusions or micro-injections of labeled proteins, have appeared recently (Kim et al. 2004, 2005; Larson et al. 2005). Live cell applications based on simultaneous two-color excitation using two coaxially aligned visible lasers have been published recently as well (Saito et al. 2004; Thews et al. 2005; Baudendistel et al. 2005). The dimerization of the ligand binding domains (LBDs) of retinoid receptors was studied in live cells by one channel photon counting histogram analysis, which is a variation of the analysis of fluctuation data (Chen et al. 2003). This group has described a two-color version of the PCH experiment (Chen et al. 2005a), recently applied to NRs LBD interactions (Chen et al. 2005b). In the present work, we describe the direct measurement of the ligand-dependent interaction between full-length eCFP-labeled AR and eYFP-labeled Tif2 in live Cos-7 cells using TPTCFCCS.

Materials and methods

Plasmids and ligands

The fusion proteins, eCFP-AR and eYFP-Tif2 were expressed by insertion of the sequences encoding AR and Tif2 in PC1-ECFP and PC2-EYFP vectors from Clontech, bearing the appropriate fluorescent protein sequence. Plasmid preps were carried out using DH5α cells grown on kanamycin. The ligands, R1881 and casodex, were the kind gift of Dr. Gordon Hager.

Cell culture and transfections

Cos-7 cells were cultured in DMEM medium (Invitrogen) supplemented with 10% fetal calf serum (Atlanta Biologicals), penicillin (100 μg/ml) and streptomycin (100 μg/ml) in a humidified atmosphere containing 5% CO_2 at 37°C. For imaging and FCS, cells were plated on chambered coverglass (0.17 mm thick) (Labtek, grown to approximately 60% confluency, then transfected with 1–2 μg total of plasmid using Fugene 6 (Roche Applied Science) and grown overnight. They were then washed several times with PBS and the medium replaced with phenol red free medium containing charcoal stripped serum. Ligands were added where necessary at a concentration of 10 nM. Hepes buffer at 10 mM was also added to help maintain the intracellular pH during imaging. Cells

were incubated with ligands for at least 2 h prior to imaging. Imaging was carried out for only 15 min at a time per sample, and during imaging unused chambers were stored in a CO_2 incubator at 37°C.

Confocal microscopy

Confocal microscopy was carried out using an LSM 510 META confocal system equipped with 405-Vis lasers from Carl Zeiss, Inc (Jena, Germany). Cells were viewed with a 63X, 1.4-numerical-aperture Plan-Apochromat oil immersion objective. Images were acquired sequentially using a 458-nm laser line and emission between 470 and 500 nm for eCFP and a 514-nm laser line and emission between 530 and 600 nm for eYFP. Overlay images were assembled using Imaris 4.0 software form Bitplane AG (Zurich, Switzerland).

TPTCCCS

Two photon imaging and FCS measurements were carried out using a system set up in the laboratory. The excitation source was a fs pulsed tunable titanium sapphire wide band Mai Tai laser (Spectra-Physics-Newport) set at 920 nm, which proved to yield the best intensity ratios between the CFP and YFP signals. In principle one would like to measure similar signal levels for each in their respective channels, 1 for YFP and 2 for CFP at similar concentrations. While we could not know, prior to the data analysis, the concentrations of the two proteins, we chose the emission filters and excitation wavelengths to yield approximately the same light levels in each channel. The excitation power was set at a level (<25 mW at the microscope entrance) below which no further increase in the correlation amplitude was observed, in order to ensure minimal photobleaching and avoid excitation saturation effects (Berland and Shen 2003). The microscope was a Zeiss Axiovert 135 using an E700 SP 2P dichroic filter (Chroma Technology Corporation) to eliminate the IR exciting light in the emission. The objective was a 100X Plan-Neofluar oil objective (Zeiss) with a 1.3 numerical aperture. The microscope was equipped with a piezo-electric stage for *x*-*y* control (ISS, Inc.) and the objective was also equipped with a piezo-electric device for *z*-control (also from ISS, Inc.). Detection was carried out using the Alba 2 channel fluorescence correlation system (ISS, Inc.) equipped with Avalanche photodiodes. A 515 nm dichroic mirror was used to split the detected light onto two channels, and an additional 550 ± 20 nm band-pass emission filter was placed before channel 1 to minimize the contribution of the eCFP signal. Excitation volumes were calibrated by measuring the diffusion of rhodamine 110 (Molecular Probes R110, Eugene OR), a 61 nM solution in water, using an excitation wavelength of 920 nm. The beam waist, w_o, recovered from the fit of the auto-correlation curve fixing the concentration to 61 nM and the diffusion coefficient to 300 μm^2/s was found to be 0.33 μm, while the z_o was 1.2 μm. The diffraction limit at 920 nm excitation wavelength with the 1.4 N.A. 100X oil objective used is ~0.4 μm. This is a bit larger than the value for w_o recovered from the fit. Therefore, the data were fit fixing the value of w_o at 0.4 μm. The resulting χ^2 was not significantly different (0.74 compared to 0.72) from that obtained in the fit performed with the value of w_o allowed to float. Thus, the volume of 0.092 fL results from alignment of the excitation optics to the diffraction limit. Correlation profiles were collected over a period of 2–3 min and raw data were only used for periods where no photobleaching was observed. In general, the FCS and imaging data on the Cos-7 cells were acquired at light levels for which photobleaching was not evident (<25 mW at the scope entrance). This precluded collecting data in regions of the cells exhibiting punctate distribution patterns of fluorescence, which exhibited very slow diffusion. Such punctate structures were particularly evident in the presence of the antagonist, casodex, as has been previously demonstrated (Karvonen et al. 2002), and these structures were avoided in data acquisition. The two-photon imaging scan rate was 1 pixel/ms.

Theory

Fluorescence fluctuations are time-correlated to generate the auto-correlation function $G(\tau)$, defined as

$$G(\tau) = \langle \delta F(t) \delta F(t+\tau) \rangle / \langle F(t) \rangle^2 \quad (1)$$

with τ, being lag time. For an ideal case of freely diffusing, monodisperse and uniformly bright fluorescent molecules, a closed form expression for Eq. 1 was derived

$$G(\tau) = (\gamma/N)(1+\tau/\tau_d)^{-1}(1+\omega_o^2\tau/z_o^2\tau_d)^{-1/2}. \quad (2)$$

The geometric factor γ, provides a measure of the uniformity of the fluorescence intensity observed for molecules at different positions within the volume and the abruptness of the boundaries of this latter. The parameters ω_o and z_o are the width and length,

respectively, of the three-dimensional Gaussian excitation volume at which the intensity drops to $1/e^2$. This expression is commonly used to analyze auto-correlation functions in terms of the diffusion time, τ_d, and the average number of molecules in the volume, N.

By exciting simultaneously two fluorophores which emit at different wavelengths, and simultaneously detecting their emission in two separate channels, i and j, under ideal conditions with no cross-talk (channel i only detects species 1 and 12 while channel j only detects species 2 and 12), the cross-correlation function then becomes:

$$G_{ij}(\tau) = \langle \delta Fi(t)\delta Fj(t+\tau)\rangle / (\langle Fi(t)\rangle\langle Fj(t)\rangle). \quad (3)$$

If we assume that the species present are the two free species, 1 and 2 and the complex 12, then Eq. 3 becomes

$$G_{ij}(\tau) = (\langle C_{12}\rangle M_{12}(\tau))/(V(\langle C_1\rangle + \langle C_{12}\rangle)(\langle C_2\rangle + \langle C_{12}\rangle)), \quad (4)$$

where C_1, C_2, and C_{12} are the concentrations of the free and interacting species, respectively, and M_{12} is the term describing the diffusion of the complex.

$$M_{12} = (1+\tau/\tau_{d12})^{-1}(1+r_o^2\tau/z_o^2\tau_{d12})^{-1/2}. \quad (5)$$

The amplitude at time 0 of the cross-correlation function is

$$G(0)x = \langle C_{12}\rangle/(V\langle C_{1T}\rangle\langle C_{2T}\rangle) \quad (6)$$

where

$$\langle C_{1T}\rangle = (\langle C_1\rangle + \langle C_{12}\rangle) \quad \text{and} \quad \langle C_{2T}\rangle = (\langle C_2\rangle + \langle C_{12}\rangle).$$

Simultaneous excitation of two fluorophores can be achieved either using two coaxially aligned laser beams of different wavelengths (Kettling et al. 1998) or alternately through two photon excitation using a femtosecond pulsed IR laser at a single wavelength (Heinze et al. 2000). The very broad two-photon cross-sections of many fluorophores are due to the different selection rules for the two-photon transition, and this permits for simultaneous excitation of fluorophores even if they exhibit large wavelength differences in their one-photon absorption peaks.

To correct for the ''bleed-through'' (cross-talk) of the CFP fluorescence signal in the YFP channel, we used the equations of Kim et al. (2005). The amplitude at time 0 of the auto-correlation correlation functions from the blue (b) and yellow (y) channels was defined respectively as

$$G(0)\mathrm{b} = \Sigma_i \eta_{i,\mathrm{b}}^2 C_i / V(\Sigma_i \eta_{i,\mathrm{b}} C_i)^2 \quad (7)$$

and

$$G(0)\mathrm{y} = \Sigma_i \eta_{i,\mathrm{y}}^2 C_i / V(\Sigma_i \eta_{i,\mathrm{y}} C_i)^2 \quad (8)$$

and the cross correlation amplitude at time 0 was

$$G(0)x = \Sigma_i(\eta_{i,\mathrm{b}}\eta_{i,\mathrm{y}} C_i)/V(\Sigma_i \eta_{i,\mathrm{y}} C_i)(\Sigma_i \eta_{i,\mathrm{b}} C_i). \quad (9)$$

The molecular brightness values, $\eta_{i,\mathrm{b}}$ and $\eta_{i,\mathrm{y}}$, of the species in each channel are taken into account, and the sums are over the three species, free eCFP-AR, free eYFP-Tif2 and the double labeled eCFP-AR/eYFP-Tif2 complex. The molecular brightness values of the eCFP and eYFP constructs in both channels were determined by separate analysis of the photon counting histograms (Chen et al. 1999) using the ISS software for data taken under identical illumination and detection conditions. Equations 7–9 were solved using the function SOLVE in Mathematica version 4.1.

Results and discussion

Visible confocal microscopy of the Cos-7 cells (chosen because they do not express endogenous AR) co-transfected with expression plasmids bearing the eCFP-AR and eYFP-Tif2 fusion proteins confirmed the known ligand-dependent localization of the AR (Black and Paschal 2004; Karvonen et al. 2002; Whitaker et al. 2004). In the absence of ligand, eCFP-AR is localized predominantly in the cytoplasm, whereas eYFP-Tif2 is nuclear (Fig. 1, Panel A). Upon addition of the agonist, R1881, eCFP-AR translocated to the nucleus as expected (Georget et al. 1997) and visually co-localized with the eYFP-Tif2 (Fig. 1, Panel B), confirming that the eCFP-AR fusion protein was competent for ligand binding. In the presence of the antagonist, casodex, this translocation of eCFP-AR occurred, but was incomplete (Fig. 1, Panel C). These observations are consistent with the previously demonstrated lower translocation efficiency of casodex (Tyagi et al. 2000) as compared to agonist ligands. The eYFP-Tif2, while remaining nuclear in presence of antagonist, formed punctate structures which have been previously reported (Karvonen et al. 2002). These punctuate structures are thought to result from partial sequestering of the co-activator in specific nuclear bodies, although their nature is not known. Two-photon images (Fig. 2) of the Cos-7 cells co-transfected with eCFP-AR and eYFP-Tif2 were similar to those obtained using visible confocal microscopy. As in the

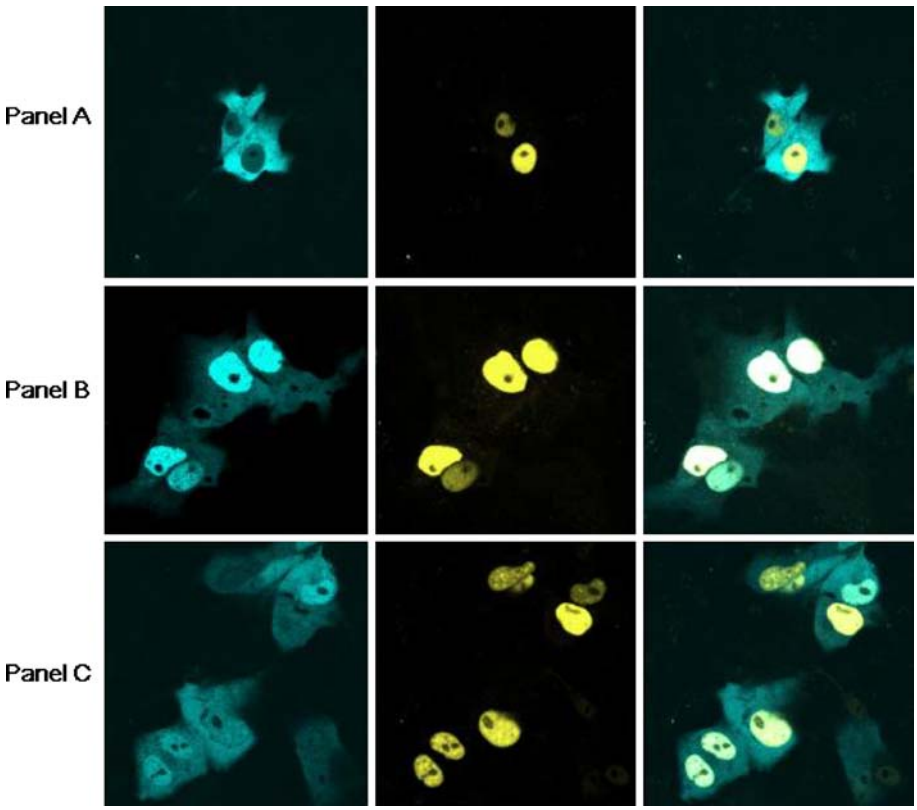

Fig. 1 Confocal images of Cos-7 cells co-transfected with eCFP-AR and eYFP-Tif2. The *first column* corresponds to the eCFP channel, the *second column* to the eYFP channel and the *third column* is a merge of the two. *Panel A* represents cells imaged in absence of any ligand, *Panel B* corresponds to images of cells in presence of 10^{-8} M of the agonist R1881, and *Panel C* corresponds to images of cells in presence of 10^{-8} M of the antagonist, casodex

one-photon images, without ligand, eCFP-AR was cytosolic, while in the presence of either ligand, eCFP-AR moved into the nucleus (albeit to different extents for agonist vs. antagonist). Again, eYFP-Tif2 was nuclear in all cases. While both eCFP-AR and eYFP-Tif2 are found in the nucleus in the presence of both agonist and antagonist ligands, their protein–protein interaction is expected to be favored in presence of agonists. To differentiate between simple visual co-localization, and true physical interaction of eCFP-AR and eYFP-Tif2, we used TPTCFCCS.

As expected for a well-aligned system, the amplitude of the cross-correlation function of the cytoplasmic signals from channels 1 and 2 (emanating solely in this case from the eCFP-AR due to cross talk) in the absence of ligand was 100% because it corresponds to eCFP-AR self-diffusion (data not shown). When only the CFP is observed, as is the case in the cytoplasm regardless of the ligation conditions, about 25% of the signal level observed in channel 2 (the CFP channel) was observed in channel 1 (the YFP channel) due to cross talk (for example, 19,500 cps in channel 1 compared to 78,600 in channel 2). On the other hand, measurement of the YFP-Tif2 construct alone showed that only 5%, of the signal in channel 1 was measured in channel 2 (5,600 counts in channel 1 compared to 275 cps in channel 2). This demonstrates that auto-fluorescence from the cells contributes very little to the signals since only 275 counts are measured in Channel 1 and the cross-correlation when only CFP is observed is almost 100%. Since the auto-fluorescence is not equal in each channel, the cross-correlation amplitude would be diminished significantly, in the event of significant auto-fluorescence contribution to the signals. Thus, our instrument is well-aligned with a diffraction limited excitation volume and very little if any contribution of background fluorescence to our signals.

Figure 3 shows examples of the auto-correlation and cross-correlation curves obtained in the nucleus of cells treated with the agonist R1881 (Fig. 3a) and the antagonist casodex (Fig. 3b). In the presence of agonist, the cross-correlation signal is essentially equal in amplitude to the lowest of the auto-correlation signals, the maximal cross-correlation achievable between the intensity fluctuations from the two channels. This, in turn, reveals a maximal degree of interaction between the two proteins. In the presence of the antagonist, the amplitude of the cross-correlation is significantly reduced relative to the lowest auto-correlation amplitude (Fig. 3b, c), consistent with a decrease in the interaction between eCFP-AR and eYFP-Tif2 when antagonist is present. While the amplitude of the cross correlation signal depends upon the total concentrations of the proteins, and thus cannot in principle be

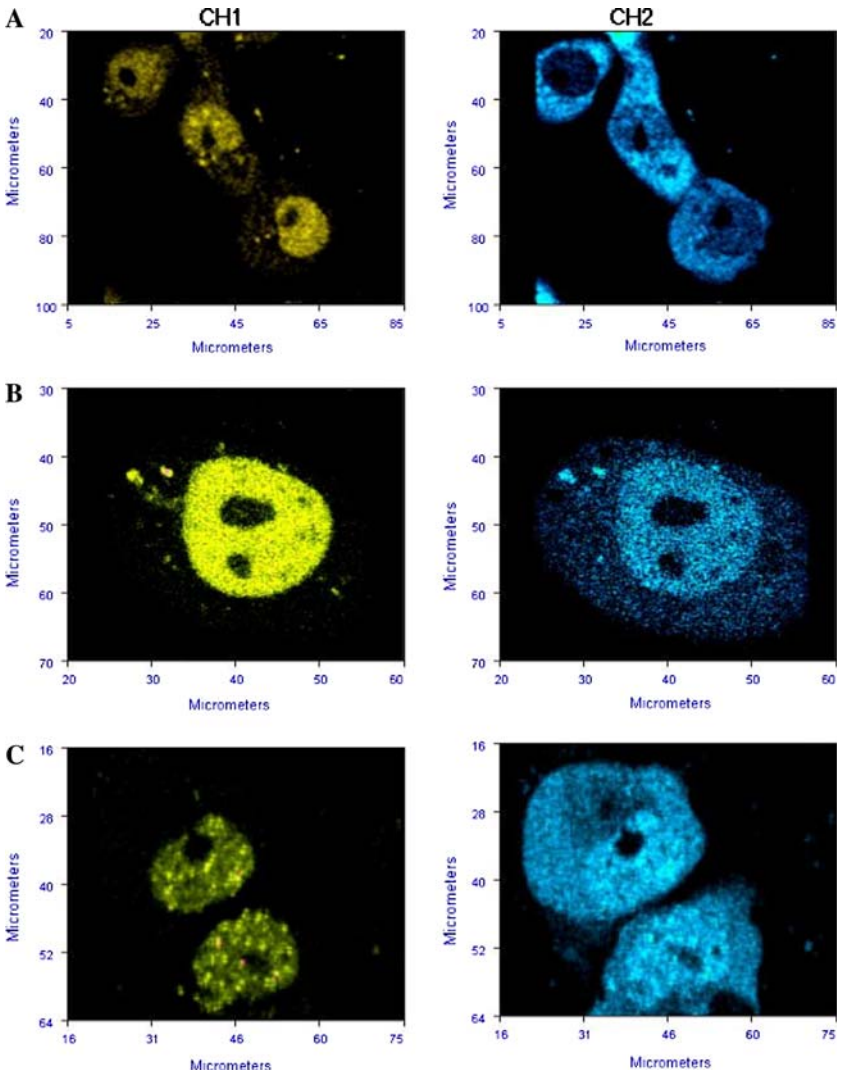

Fig. 2 Two-photon images of Cos-7 cells co-transfected with eCFP-AR and eYFP-Tif2. The *first column* corresponds to the eYFP channel, the *second column* to the eCFP channel. *Panel A* corresponds cells in absence of any ligand, *Panel B* corresponds to images of cells in presence of 10^{-8} M of the agonist R1881, and *Panel C* corresponds to images of cells in presence of 10^{-8} M of the antagonist, casodex. The excitation wavelength was 920 nm

compared directly from one experiment to the next, here the concentrations of the most concentrated species in Fig. 3a, b are quite close (Go of CH1 is about 0.006 in Fig. 3a and 0.0052 in Fig. 3b) and so in this case direct comparison of the cross correlation signals is possible between the two data sets.

In principle, from the values of the auto and cross-correlation amplitudes at time zero, one can quantitatively determine the degree of interaction between the two proteins according to Eq. 5 (Kim et al. 2005). The fluorescence detected in channel 1, however, includes intensity from both eCFP-AR and eYFP-Tif2. This bleed-through could lead to an overestimation of the concentration of eYFP-Tif2. Cells were chosen for imaging based on the high count-rate in channel 1 (predominantly eYFP) relative to that in channel 2 (eCFP) in order to limit this effect. For example, for the data in Fig. 3a, the total intensity in the eCFP channel 2 was nearly fourfold lower than that in the intensity in the eYFP channel l. In this situation, the bleed-through from eCFP into the eYFP channel amounted to only 10% of the total signal in the eYFP channel.

If one knows the molecular brightness of each species in each channel in counts per second per molecule (cpspm), then the actual concentrations of the species can be calculated by solving Eqs. 7–9. The molecular brightness of the eCFP in both channels was determined by separate analysis of the photon counting histograms (Chen et al. 1999) derived from the photon fluxes of the emission from the cytoplasm. Since the eYFP-Tif2 is nuclear under all conditions, the signal from the cytoplasm in both channels arises only from eCFP-AR. The molecular brightness for eCFP-AR in the blue channel as determined by PCH analysis was 16,040 cpspm, and in the yellow channel, 3,850 cpspm. For eYFP, the molecular brightness in the yellow channel was determined from the PCH analysis of the photon flux from data taken in the nucleus in absence

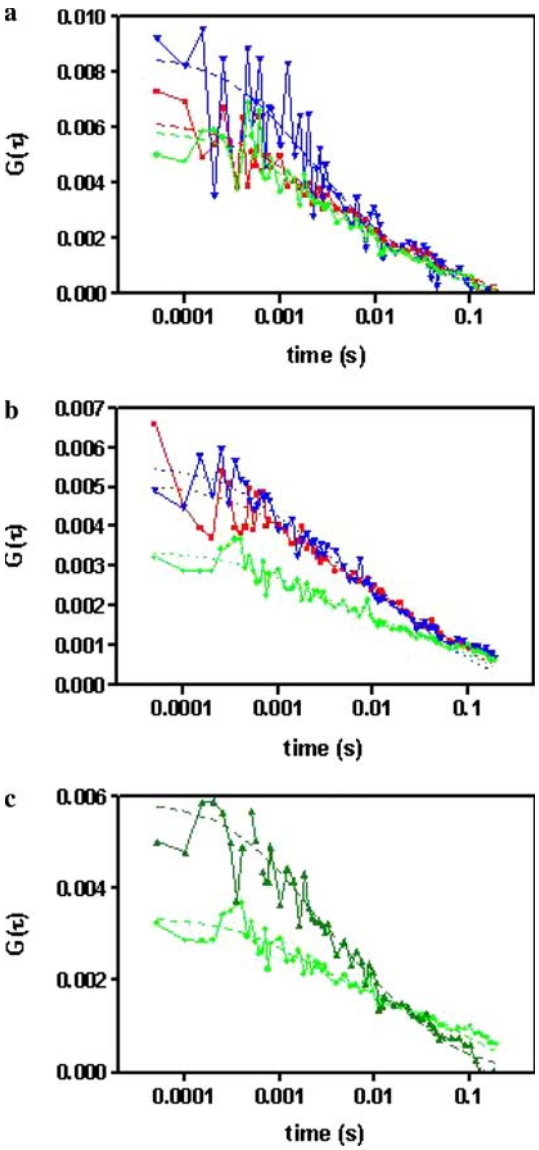

Fig. 3 Auto functions of the emission in the eYFP (channel 1, *red*) and eCFP (channel 2, *blue*) channels, and cross-correlation functions (Channel1 X channel2, *green*) for two-photon excitation of Cos-7 cells co-transfected with eCFP-AR and eYFP-Tif2. **a** Curves correspond to profiles calculated from to data obtained in the nucleus in presence of 10^{-8} M R1881 (Fig. 2, Panel B), **b** curves correspond to profiles calculated from to data obtained in the nucleus in presence of 10^{-8} M casodex (Fig. 2, Panel C), and **c** the cross-correlation profiles from **a** (*upper curve*, *dark green*) and **b** (*lower curve*, *light green*) are re-plotted for direct comparison. Excitation was at 920 nm

of ligand to be 36,371 cpspm. In this case there is negligible eCFP contribution to the yellow channel, because very little eCFP-AR is localized in the nucleus in the absence of ligand. It was assumed for subsequent calculations that the brightness values of the eCFP and eYFP fluorescent proteins were unaltered by the formation of the complex. We note that previous studies using acceptor-bleaching methods indicated little or no FRET in this eCFP-AR/eYFP-Tif2 system under any conditions of ligation (V. Georget and J.C. Nicolas, unpublished results). Moreover, the fluorescent proteins contain fluorophores in a protected environment and do not participate in the structure of the receptor, but rather are attached by a peptide linker to the N-terminus. They are much less likely than a small covalently attached dye molecule (Kim et al. 2004, 2005) to be quenched by changes in protein structure accompanying interactions. We also assumed that the eYFP did not contribute significantly to the blue channel, given its red-shifted spectrum.

The concentrations of the eCFP-AR and eYFP-Tif2 for the data in Fig. 3 are given in Table 1, along with those corresponding to analysis of FCS data obtained for several different cells under different ligation conditions. In total the data used for the results given in Table 1 were collected from two different transfection experiments using four different cells in six different FCS acquisitions in presence of antagonist and from seven different cells in seven different acquisitions for the agonist. The total concentrations of eCFP-AR and eYFP-Tif2 vary by a factor of about 20–30 for the different cells imaged. The fractional complex formation is calculated with respect to the species of lowest total concentration (the limiting partner). On average for all of the cells imaged, the degree of binding is 81 ± 9% in presence of agonist and 56 ± 5% in presence of antagonist.

The time-dependence of both the auto and cross-correlation functions was clearly heterogeneous. The auto and cross-correlation curves could be reasonably well fit in all cases using two diffusing species, one reasonably fast, between 5 and 7 $\mu m^2/s$, and the other about tenfold slower, and while the contributions of the two times was ligand dependent, no obvious difference in diffusion times could be observed as a function of ligation state. Distinguishing by diffusion times complexes that differ by a factor of 2 in their molecular weight is possible, although difficult, in vitro, but the heterogeneous nature of the intra-cellular environment precludes such sophisticated analysis. This underscores the difficulty of interpreting diffusion in live cells, and reinforces that notion that Go, the amplitude at time 0 of the cross-correlation signal can be more reliable for determining complex formation than time-dependence. Thus, we do not attach any particular meaning to the diffusion coefficients extracted from analysis of the correlation curves. The diffusion is likely to be much more complex than the model used, which was simply the least complicated model that adequately describes the data.

Table 1 Free protein and complex concentrations derived from analysis of the correlation amplitudes

[CFP-AR] (μM)	[YFP-Tif2] (μM)	[Complex] (μM)	% Complex $[AR]_{total}$	% Complex $[Tif2]_{total}$
Agonist (Figs. 2b, 3a)				
0.4	1.8	3.5	90.3	
6.8	1.9	5.5		75
1.8	0.2	0.6		76
8.4	4.0	8.2		68
3.0	10.0	12.8	81	
3.0	0.5	1.8		75
3.0	0.1	2.2		95
Antagonist (Figs. 2c, 3b)				
3.3	2.7	2.8		50
4.0	1.8	2.2		55
5.9	1.7	2		54
6.2	1.7	1.9		53
4.9	1.2	2.3		65
8.8	4.1	5.1		56

Conclusions

We provide here direct, quantitative measurements of the ligand-dependent interaction between AR and one of its physiological co-activators, Tif2, in live cells. FCCS measurements are more reliable than FRET, since they do not depend upon absolute or relative intensities or quaternary structures with inter-fluorophore distances within 7 nm. Interestingly, we find in the present work that, in the presence of antagonist, the interaction between AR and Tif2 is not abolished. It has been shown that while the AF2 (Activation function 2) of the AR LBD is relatively weak, it nonetheless binds to SRC-1, another member of the p160 co-activor family, via the LXXLL motifs of SRC-1 in an agonist-dependent fashion (Powell et al. 2004). Mutational studies of the AF2 region of AR indicate that it exists in a dynamic conformational equilibrium that is modulated by ligands (Georget et al. 2005). Thus, even when bound be antagonist, an interaction with a co-activator remains possible. Moreover, in the absence of the LBD, the N-terminal AF1 of AR interacts with SRC-1 in a ligand-independent manner through the glutamine-rich motif present in the AR N-terminus (Powell et al. 2004). It has also been demonstrated that anti-androgen resistance in prostate cancer can be linked to over-expression of AR, thereby squelching the NCoR, and causing even Selective AR Modulators to act as agonists (Baek et al. 2006; Chen et al. 2004; Zhu et al. 2006). The significant degree of AR/Tif2 complex formation we observe in presence of the antagonist, casodex, is not surprising in the light of this complex behavior, particularly given the micromolar concentrations in the present transfection experiments.

The possibility of performing quantitative determination of protein–protein complex formation in living cells in response to the addition of a drug opens large avenues of study for the therapeutic targets where protein–protein interactions play an important role. Such studies will be clearly useful in the detailed characterization of the structure-function relationships underlying the activity of pharmaceutics or other ligands. Such measurements could be used to determine the effective concentration of drugs in various cellular compartments, via their ability to promote or to abolish complex formation, as the case may be. It may also be possible to infer the influence of protein or other co-factors necessary for ligand function using TPTCFCCS. Expression levels of endogenous proteins could be determined, as well, through competition assays with the fluorescent proteins. In any case, given the importance of investigating the interactions of NRs with their multiple partners in the cellular environment, we expect that this relatively new technique (which allows direct access to free and bound concentrations in any desired cellular location) will prove to be extremely useful in investigating the functional mechanisms of ligand dependent transcription factors.

Acknowledgments This work was supported by intra-mural funding to the investigators through the NIH and the INSERM. The authors would like to sincerely thank Dawn Walker, Gordon Hager, Cem Elbi and Bill DeGraff for their assistance in cell culture and transfections, as well as for stimulating discussions.

Reference

Bacia K, Majoul IV, Schwille P (2002) Probing the endocytic pathway in live cells using dual-color fluorescence cross-correlation analysis. Biophys J 83:1184–1193

Bacia K, Kim SA, Schwille P (2006) Fluorescence cross-correlation spectroscopy in living cells. Nat Methods 3:83–89

Baek SH, Ohgi KA, Nelson CA, Welsbie D, Chen C, Sawyers CL, Rose DW, Rosenfeld MG (2006) Ligand-specific allosteric regulation of coactivator functions of androgen receptor in prostate cancer cells. Proc Natl Acad Sci USA 103(9):3100–3105

Baudendistel N, Muller G, Waldeck W, Angel P, Langowski J (2005) Two-hybrid fluorescence cross-correlation spectroscopy detects protein-protein interactions in vivo. Chemphyschem 6:984–990

Berland K, Shen G (2003) Excitation saturation in two-photon fluorescence correlation spectroscopy. Appl Opt 42:5566–5576

Black BE, Paschal BM (2004) Intranuclear organization and function of the androgen receptor. Trends Endocrinol Metab 15:411–417

Burnstein KL (2005) Regulation of androgen receptor levels: implications for prostate cancer progression and therapy. J Cell Biochem 95:657–669

Chang C, Chen YT, Yeh SD, Xu Q, Wang RS, Guillou F, Lardy H, Yeh S (2004) Infertility with defective spermatogenesis

and hypotestosteronemia in male mice lacking the androgen receptor in Sertoli cells. Proc Natl Acad Sci USA 101:6876–6881

Chen Y, Muller JD, So PT, Gratton E (1999) The photon counting histogram in fluorescence fluctuation spectroscopy. Biophys J 77:553–567

Chen Y, Wei LN, Muller JD (2003) Probing protein oligomerization in living cells with fluorescence fluctuation spectroscopy. Proc Natl Acad Sci USA 100:15492–15497

Chen CD, Welsbie DS, Tran C, Baek SH, Chen R, Vessella R, Rosenfeld MG, Sawyers CL (2004) Molecular determinants of resistance to antiandrogen therapy. Nat Med 10:33–39

Chen Y, Tekmen M, Hillesheim L, Skinner J, Wu B, Muller JD (2005a) Dual-color photon-counting histogram. Biophys J 88:2177–2192

Chen Y, Wei LN, Muller JD (2005b) Unraveling protein-protein interactions in living cells with fluorescence fluctuation brightness analysis. Biophys J 88:4366–4377

Culig Z, Comuzzi B, Steiner H, Bartsch G, Hobisch A (2004) Expression and function of androgen receptor coactivators in prostate cancer. J Steroid Biochem Mol Biol 92:265–271

d'Ancona FC, Debruyne FM (2005) Endocrine approaches in the therapy of prostate carcinoma. Hum Reprod Update 11:309–317

De Gendt K, Swinnen JV, Saunders PT, Schoonjans L, Dewerchin M, Devos A, Tan K, Atanassova N, Claessens F, Lecureuil C, Heyns W, Carmeliet P, Guillou F, Sharpe RM, Verhoeven G (2004) A Sertoli cell-selective knockout of the androgen receptor causes spermatogenic arrest in meiosis. Proc Natl Acad Sci USA 101:1327–1332

Edwards J, Bartlett JM (2005a) The androgen receptor and signal-transduction pathways in hormone-refractory prostate cancer. Part 1. Modifications to the androgen receptor. BJU Int 95:1320–1326

Edwards J, Bartlett JM (2005b) The androgen receptor and signal-transduction pathways in hormone-refractory prostate cancer. Part 2. Androgen-receptor cofactors and bypass pathways. BJU Int 95:1327–1335

Georget V, Lobaccaro JM, Terouanne B, Mangeat P, Nicolas JC, Sultan C (1997) Trafficking of the androgen receptor in living cells with fused green fluorescent protein-androgen receptor. Mol Cell Endocrinol 129:17–26

Georget V, Bourguet W, Lumbroso S, Makni S, Sultan C, Nicolas JC (2005) Glutamic acid 709 substitutions highlight the importance of the interaction between androgen receptor helices H3 and H12 for androgen and antiandrogen actions. Mol Endocrinol 20(4):724–734

Haustein E, Schwille P (2004) Single-molecule spectroscopic methods. Curr Opin Struct Biol 14:531–540

Heinze KG, Koltermann A, Schwille P (2000) Simultaneous two-photon excitation of distinct labels for dual-color fluorescence crosscorrelation analysis. Proc Natl Acad Sci USA 97:10377–10382

Karvonen U, Janne OA, Palvimo JJ (2002) Pure antiandrogens disrupt the recruitment of coactivator GRIP1 to colocalize with androgen receptor in nuclei. FEBS Lett 523:43–47

Kettling U, Koltermann A, Schwille P, Eigen M (1998) Real-time enzyme kinetics monitored by dual-color fluorescence cross-correlation spectroscopy. Proc Natl Acad Sci USA 95:1416–1420

Kim SA, Heinze KG, Waxham MN, Schwille P (2004) Intracellular calmodulin availability accessed with two-photon cross-correlation. Proc Natl Acad Sci USA 101:105–110

Kim SA, Heinze KG, Bacia K, Waxham MN, Schwille P (2005) Two-photon cross correlation analysis of intracellular reactions with variable stoichiometry. Biophys J 88:4319–4336

Larson DR, Gosse JA, Holowka DA, Baird BA, Webb WW (2005) Temporally resolved interactions between antigen-stimulated IgE receptors and Lyn kinase on living cells. J Cell Biol 171:527–536

Lonard DM, O'Malley BW (2005) Expanding functional diversity of the coactivators. Trends Biochem Sci 30:126–132

Nettles KW, Greene GL (2005) Ligand control of coregulator recruitment to nuclear receptors. Annu Rev Physiol 67:309–333

Powell SM, Christiaens V, Voulgaraki D, Waxman J, Claessens F, Bevan CL (2004) Mechanisms of androgen receptor signalling via steroid receptor coactivator-1 in prostate. Endocr Relat Cancer 11:117–130

Saito K, Wada I, Tamura M, Kinjo M (2004) Direct detection of caspase-3 activation in single live cells by cross-correlation analysis. Biochem Biophys Res Commun 324:849–854

Smith CL, O'Malley BW (2004) Coregulator function: a key to understanding tissue specificity of selective receptor modulators. Endocr Rev 25:45–71

Thews E, Gerken M, Eckert R, Zapfel J, Tietz C, Wrachtrup J (2005) Cross talk free fluorescence cross-correlation spectroscopy in live cells. Biophys J 89:2069–2076

Tyagi RK, Lavrovsky Y, Ahn SC, Song CS, Chatterjee B, Roy AK (2000) Dynamics of intracellular movement and nucleocytoplasmic recycling of the ligand-activated androgen receptor in living cells. Mol Endocrinol 14:1162–1174

Whitaker HC, Hanrahan S, Totty N, Gamble SC, Waxman J, Cato AC, Hurst HC, Bevan CL (2004) Androgen receptor is targeted to distinct subcellular compartments in response to different therapeutic antiandrogens. Clin Cancer Res 10:7392–7401

Wu RC, Smith CL, O'Malley BW (2005) Transcriptional regulation by steroid receptor coactivator phosphorylation. Endocr Rev 26:393–399

Xu J, Li Q (2003) Review of the in vivo functions of the p160 steroid receptor coactivator family. Mol Endocrinol 17:1681–1692

Zhu P, Baek SH, Bourk EM, Ohgi KA, Garcia-Bassets I, Sanjo H, Akira S, Kotol PF, Glass CK, Rosenfeld MG, Rose DW (2006) Macrophage/cancer cell interactions mediate hormone resistance by a nuclear receptor derepression pathway. Cell 124:615–629